Surface molecular anchoring in microconfined liquid crystals near the nematic–smectic-A transition

R. J. Ondris-Crawford, G. P. Crawford, J. W. Doane, and S. Žumer*
Liquid Crystal Institute and Department of Physics, Kent State University, Kent, Ohio 44242-0001

M. Vilfan and I. Vilfan
J. Stefan Institute, University of Ljubljana, Jamova 39, 61111 Ljublana, Slovenia
(Received 23 April 1993)

The effect of the diverging bend elastic constant, K_{33}, on the nematic director field of 4′-octylcyanobiphenyl (8CB) in submicrometer cylindrical cavities in a polycarbonate matrix, as the nematic–smetic-A phase transition is approached, is investigated with deuteron nuclear magnetic resonance (^{2}H-NMR). The ^{2}H-NMR spectra and the use of Frank elastic theory enable us to monitor the actual surface anchoring angle profile, determine the density of point defects in the escaped structure, and estimate the anchoring strength to be $W_\theta = 7\times10^{-4}$ J/m^2, which is temperature independent. The large value of W_θ and the lack of evidence for pretransitional smectic layering in our NMR spectra show that although the orientational anchoring is strong, the polycarbonate surface is too rough to induce substantial surface smectic order in the nematic phase. The saddle-splay elastic constant K_{24} for 8CB is estimated to be larger than the elastic constant K_{11}.

PACS number(s): 68.10.Cr, 61.30.−v, 64.70.Md, 76.60.Gv

I. INTRODUCTION

Nematic liquid crystals confined to cylindrical cavities with homeotropic anchoring were first studied in detail by Cladis and Kleman [1], Meyer [2], and Saupe [3]. The existence of the escaped-radial (ER) structure (Fig. 1), a radial director field where the line disclination "escapes" along the cylinder axis, was first predicted in the early 1970s to appear in cylinder sizes larger than 0.1 μm. In diameters less than 0.1 μm, the planar-radial (PR) configuration was expected to become stable [1]. Optical verification of the ER configuration was obtained for cylinder sizes ranging from 200 to 2 μm [2–7] in diameter. These studies revealed the existence of singular point defects along the cylinder axis, formed as a consequence of the equivalence of the two possible escape directions of the director field.

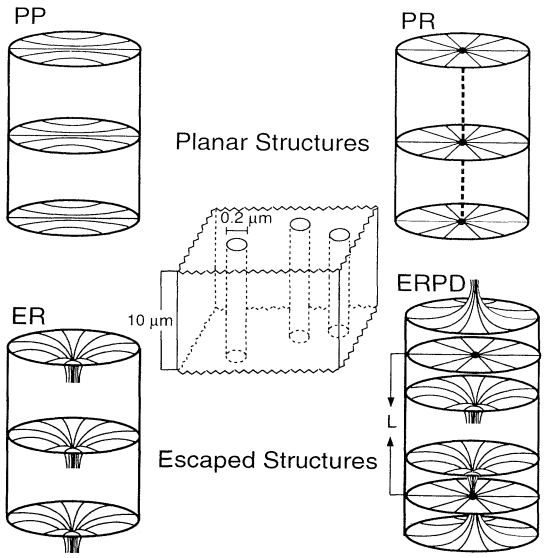

FIG. 1. Possible nematic director fields in cylindrical cavities designated as planar polar (PP), planar radial (PR), escaped radial (ER), and escaped radial with point defects (ERPD). A schematic representation of a Nuclepore membrane in shown in the center.

Recently, experimental studies on cylindrically confined nematics were extended to submicrometer radii using polycarbonate membranes with cylindrical cavities [8]. Deuterium nuclear magnetic resonance (^{2}H-NMR) was used to probe the details of the director field that are very sensitive to the molecular anchoring strength and the saddle-splay elastic constant [9–11]. The bulk elastic energy becomes relatively more important than the surface energy for decreasing cavity size, and according to elastic theory [11], if elastic constants are comparable, the director field tends toward the planar-polar (PP) structure (Fig. 1). Deuterium NMR line shapes were used to confirm the planar-polar structure for radii less than 0.4 μm, and the escaped-radial configuration with point defects (ERPD), as the cavity radius was increased above 0.5 μm (Fig. 1). Theoretical and experimental efforts by Vilfan, Vilfan, and Žumer [12] on the stability of point defects in the escaped-radial configuration extended the understanding of defect-defect annihilation and repulsion occurring in cylindrical tubes.

Optical studies of the smectic-A phase confined to supramicrometer cylindrical cavities ($R = 25$–500 μm) have been reported by Cladis [13]. Because of the divergence of the bend elastic constant K_{33} on approaching the nematic–smectic-A transition [14], areas in the sam-

ple with predominantly splay deformation increase until the structure becomes completely planar-radial (PR, Fig. 1). This enables the formation of concentric layers with respect to the cavity wall.

Smectic layering is known to propagate away from an interface before the bulk smectic-A phase transition is reached. Rosenblatt [15] observed an increase in the Fréedericksz critical field strength, in a thin planar cell with homeotropic anchoring conditions, as the nematic–smectic-A transition temperature was approached from above. The critical field is the field strength at which a Fréedericksz transition occurs when the magnetic field is applied perpendicular to the director of an aligned nematic liquid crystal in a planar cell. He attributed this to pretransitional smectic layering propagating away from the solid surfaces. Pershan and Nielsen [16] have reported x-ray-reflectivity measurements that demonstrate surface-induced smectic layering. Using the same experimental technique, Ocko has demonstrated that smectic layers propagate away from solid surfaces when the isotropic–smectic-A phase transition is approached from above [17].

The effect of finite molecular anchoring and the pretransitional divergence of the bend elastic constant on nematic director-field configurations is the focus of this paper. To observe this effect experimentally a liquid-crystal material which possesses a nematic–smectic-A phase transition was confined to polycarbonate membranes with cylindrical cavities of diameter 0.2 μm. The resulting director configurations were studied with ^{2}H-NMR as the smectic-A phase was approached from above. This paper will first review the materials in Sec. II and discuss the application of elastic theory to our systems in Sec. III. Section IV is devoted to the application of the NMR technique to confined liquid crystals, with the experimental results following in Sec. V. We conclude in Sec. VI.

II. MATERIALS

The liquid-crystal material 4′-octyl-4-cyanobiphenyl deuterated in the β position of the hydrocarbon chain (8CB-βd_2) is used in this study. The bulk phase transition temperatures upon cooling of this compound, observed with a polarizing optical microscope are [18] isotropic-nematic: 40.3 °C; nematic–smectic-A: 33.1 °C; and smectic-A–crystal: −2.2 °C.

The porous polycarbonate, poly(carbonyldioxy-1,4-phenyleneisopropylidene-1,4-phenylene), membranes used for this study are Nuclepore membranes [19]. Scanning electron microscopy photographs of Nuclepore membranes are available in the literature [20,21]. The large amount of pores in the membranes (pore density of 3×10^8 cm^{-2}) are etched to the desired dimension from damaged radiation tracks. Kuzma and Labes [22] have used optical polarizing microscopy on polycarbonate membranes filled with various liquid crystals to confirm homeotropic anchoring at the surface. A schematic diagram of the cylindrical cavities is shown in the center of Fig. 1. The pore radius of 0.1 μm is a nominal pore size with 80% of the pore radii in this filter being within 10% of the mean [21]. The cylindrical cavities are parallel to the membrane's normal and extend through the entire 10-μm-thick membrane.

The 8CB-βd_2 liquid-crystal material was heated to the isotropic phase and introduced into 5-mm-wide Nuclepore membrane strips. To attain the desired signal-to-noise ratio of the NMR experiment, 250 membrane strips were prepared in this manner and stacked uniformly on top of each other. The sample was then carefully placed in an NMR sample tube. Angular-dependent studies of the small cavities with respect to the magnetic field of the NMR spectrometer were possible by rotating the sample in the probe by a stepper motor.

III. SIMULATED STRUCTURES

The nematic director field inside a small cavity under stable conditions depends on the elastic properties of the liquid-crystal material, the strength of an external magnetic (or electric) field, and the preferred orientation of the molecular anchoring at the cavity wall [23]. If the typical dimension (here cylinder radius) is much larger than the nematic coherence length [6], and assuming a constant nematic order parameter, stable director fields can be determined for these systems using the free energy associated with the deformation of the director field. In our system this is well justified except in dealing with singular disclination lines and pretransitional smectic ordering. The simplified free energy includes bulk elastic and surface elastic terms, the orientational surface anchoring contribution, the magnetic-field coupling, and a smectic layering term, and is expressed as

$$F=\tfrac{1}{2}\int_{\text{vol}}\{K_{11}(\nabla\cdot\mathbf{n})^2+K_{22}(\mathbf{n}\cdot\nabla\times\mathbf{n})^2+K_{33}(\mathbf{n}\times\nabla\times\mathbf{n})^2-K_{24}\nabla\cdot(\mathbf{n}\times\nabla\times\mathbf{n}+\mathbf{n}\nabla\cdot\mathbf{n})\}dV$$
$$+\tfrac{1}{2}\int_{\text{surf}}W_\theta\sin^2\theta\,dS-\frac{\Delta\chi}{\mu_0}\int_{\text{vol}}(\mathbf{B}\cdot\mathbf{n})^2dV+\tfrac{1}{2}\int_{\text{vol}}D\theta^2dV\ . \tag{1}$$

Here K_{11}, K_{22}, K_{33}, and K_{24} are the well-known bulk elastic constants associated with the splay, twist, bend and saddle-splay deformations, respectively, and $\mathbf{n}$ is the nematic director. The interaction between the elongated liquid-crystal molecules and the cavity wall is modeled after the simple Rapini-Poupular form [24] characterized by the polar molecule anchoring strength, W_θ, with θ depicting the angle between the director and the direction normal to the cavity surface. The magnetic-field term depends on $\Delta\chi$, the anisotropy in the diamagnetic susceptibility. The influence of the magnetic field of the NMR spectrometer (4.7 T) on the director field is negligible, since the magnetic coherence length, $\xi_i=(1/B)[\mu_0K_{ii}/\Delta\chi]^{1/2}>1.5$ μm, is substantially larger

than the radius ($R=0.1$ μm) of our cavities for reported values of the Frank elastic constants, K_{ii}, and the diamagnetic susceptibility, $\Delta\chi$; therefore, the influence of the magnetic-field term is neglected in our calculations of the director field and free energy. The last term describes the contribution of the smectic ordering and is expected to be nonzero only in cases when, upon approaching the nematic–smectic-A phase-transition temperature T_{NA}, surface-induced smectic layering appears [15]. We take into account only the elastic energy which originates from the deviation of the nematic director from the direction normal to the smectic layers [15]. According to Landau theory [25], the coefficient D is assumed to be proportional to the square of the smectic order parameter, Ψ, which in the case of the second-order phase transition decreases exponentially ($e^{-z/\xi}$) with the distance from the surface, z. The critical behavior of the characteristic correlation length, ξ, can be described as $\xi \propto |T-T_{NA}|^{-\nu}$ [25], where $\nu=0.65$. If we are not too close to T_{NA}, [$\xi(T_{NA}+0.1K)\sim 0.1$ μm], the volume integral $\frac{1}{2}\int D\theta^2 dV$ can be reduced to $\frac{1}{2}\int D_{surf}\frac{1}{2}\xi\, dS$ with $D_{surf}=D(\Psi_{surf})$. This means that effectively the surface orientational anchoring strength W_θ is renormalized to $W_\theta+\frac{1}{2}D_{surf}\xi$. The additional term has a critical behavior which depends on the strength of the positional anchoring of the liquid-crystal molecules on the surface. For instance, if the surface strongly induces smectic order (strong positional anchoring) then Ψ_{surf} is expected to be constant, and the entire critical dependence of this additional orientational anchoring is determined by ξ. For weaker coupling, however, one would expect an increase in Ψ on approaching T_{NA}, thus resulting in a stronger temperature dependence of the additional orientational anchoring. This simplified approach, resulting in the renormalization of the orientational anchoring strength, will be sufficient for the analysis of the possible occurrence of smectic layering in our system.

The planar-radial (PR) structure (Fig. 1) is the simplest configuration to conceive [13,26]. Since **n** is always normal to the surface, there is no anchoring energy associated with the deviation from the homeotropic director field. The pure splay deformation yields a free energy per unit length:

$$F_{PR}/l=\pi K_{11}[\ln(R/\rho)+\tfrac{1}{2}] \ . \tag{2}$$

Here the divergent splay energy in the center of the cylinder is relieved by simply assuming an isotropic core disclination line of radius ρ. Equation (2) is a result of an approximation of the total free-energy density which consists of the elastic free-energy density, $f_e=\frac{1}{2}K_{11}(1/r^2)$, and the intrinsic free-energy density of the nematic phase, $f_N\sim\frac{1}{2}AS^2$, where $A=a(T-T^*)S^2$ is a phenomenological constant in the Landau–de Gennes description [6]. For the nematic phase to exist the total free-energy density, f_e+f_N must be <0, while the isotropic phase is preferred when $f_e+f_N>0$. At the isotropic core radius, therefore, $f_e=-f_N$. This yields $\frac{1}{2}\pi K_{11}$ for the contribution of the core to the deformation free energy, and $\rho\sim 0.005$ μm for the core radius, (using $a=0.13\times 10^6$ J/m^3 K, $T-T^*=-10$ K, $S=0.6$, and $K_{11}\sim 10^{-11}$ J/m). A more detailed analysis of the calculation of the core radius and its contribution to the free energy is available in the literature [7].

The other well-known solution of the minimization of the free energy, the escaped-radial (ER) structure (Fig. 1), yields [10]

$$\begin{aligned}\frac{r}{R}=&\left[\left[\frac{\sigma+1}{\sigma-1}\right]\left[\frac{\Delta-\beta'\cos\Omega(r)}{\Delta+\beta'\cos\Omega(r)}\right]\right]^{1/2}\\ &\times\exp\left[\frac{\beta}{\beta'}\sin^{-1}(\beta\cos\Omega_R)\right]\\ &\times\exp\left[-\frac{\beta}{\beta'}\sin^{-1}(\beta\cos\Omega(r))\right],\\ k\equiv K_{33}/K_{11}>1\ ,&\end{aligned} \tag{3}$$

where $\sigma=RW_\theta/K_{11}+K_{24}/K_{11}-1$ is the dimensionless surface parameter, $\beta^2=|k-1|/k$, $\beta'^2=1/k$, and $\Delta=[1-\beta^2\cos^2\Omega(r)]^{1/2}$. The angle $\Omega(r)$ is the angle between the local nematic director **n** and the cylinder axis, and the molecular anchoring angle $\Omega_R=\Omega(r=R)=\cos^{-1}[k/(\sigma^2+k-1)]^{1/2}$ is evaluated at $r=R$. It should be noted that $\Omega=\pi/2-\theta$, where θ is the angle in Eq. (1), was chosen in order to stay consistent with the notation for the ER structure reported in the literature [9–11]. A more detailed presentation of the influence of the effective surface anchoring parameter σ and the bend-to-splay elastic constant ratio K_{33}/K_{11} on the local director orientation $\Omega(r)$ is shown in Fig. 2; the top surface represents the weak anchoring regime ($\sigma=4$) and the bottom surface corresponds to the strong anchoring regime ($\sigma=\infty$). The costly bend (increasing K_{33}) elastic energy is relieved by decreasing the area with strong bend. The manner in which this is reduced depends on the anchoring regime. For infinitely strong anchoring and large values of K_{33}/K_{11}, the angle the nematic director makes with respect to the surface remains large until close to the cylinder axis, where it decreases rapidly until

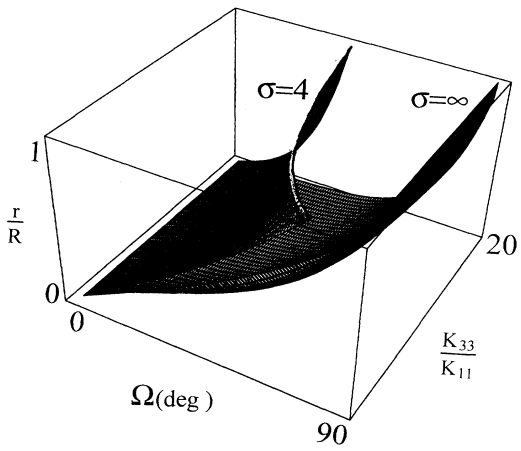

FIG. 2. The nematic director distribution given by Eq. (3) describing the escaped-radial configuration in terms of K_{33}/K_{11} in weak ($\sigma=4$) and strong ($\sigma=\infty$) anchoring regimes.

the director is parallel to the cylinder axis. Thus the escaped region in the center is reduced while keeping the molecular anchoring angle Ω_R perpendicular to the surface. For strong anchoring and values of K_{33}/K_{11} close to unity, Ω decreases gradually from the cylinder radius to the center. For weak anchoring ($\sigma=4$) the expensive bend elastic energy is reduced by decreasing the molecular anchoring angle at the cavity wall.

Substituting the nematic director field of the escaped-radial structure into the equation for the free energy Eq. (1) and neglecting the field contribution, the free energy for $k>1$ was previously calculated to be [10]

$$F_{\mathrm{ER}}/l=\pi K_{11}\left[2+\frac{k}{\sqrt{k-1}}[\tan^{-1}\sqrt{k-1}-\tan^{-1}(\sqrt{k-1}/\sigma)]-\frac{K_{24}}{K_{11}}\right]. \quad (4)$$

It should be noted that the configuration transition between the escaped-radial structure and the planar-radial structure for diverging K_{33}/K_{11}, first observed by Cladis [13], in the strong anchoring regime depends on the saddle-splay surface elastic constant K_{24}. The R/ρ $-K_{33}/K_{11}$ phase diagram for the PR and ER in the strong anchoring regime presented in Fig. 3(a) illustrates this point. The diagram is prepared by equating Eqs. (2) and (4). By carefully measuring the configurational transition temperature (which corresponds to a specific value of K_{33}/K_{11}), the value of K_{24} can be estimated. The phase diagram in Fig. 3(b) shows the stability of the PR and ER structures for the effective anchoring strength of $\sigma=12$. This diagram shows that the lines separating the area of stability for the different structures have been shifted down in comparison with those of the strong anchoring regime [Fig. 3(a)]. The inset in Fig. 3(b) represents the stability of the ER, PR, and PP structures as a function of the elastic constant ratio K_{33}/K_{11} and shows the existence of a triple point. The PP structure for nonequal elastic constants was previously reported numerically [27]. This ER-PR-PP stability diagram, calculated for $\sigma=12$ and $K_{24}/K=1.0$, shows the theoretical possibility of the reentrance of the PP structure from the ER structure upon approaching the smectic-A phase (increasing K_{33}/K_{11}). The experimental evidence for this reentrance is yet to be seen. In our case, the value of R/ρ is ~ 20 for $R=0.1$ μm, and $\rho\sim 0.005$ μm.

One must not forget that this diagram corresponds to an idealized situation with ER being a perfect escaped director field. The real systems, first observed using optical microscopy [2–5], usually exhibit a number of point defects along the symmetry axis of the ER structures. These defects may appear when cooling from the isotropic to nematic phase and are caused by the configuration escaping in both (energetically equivalent) directions along the cylinder axis [12]. This may be caused by fluctuations near the N-I transition, irregularities of the cavity wall, or by conditions imposed by both ends of the cylinder. In ideal infinite cylindrical cavities, the

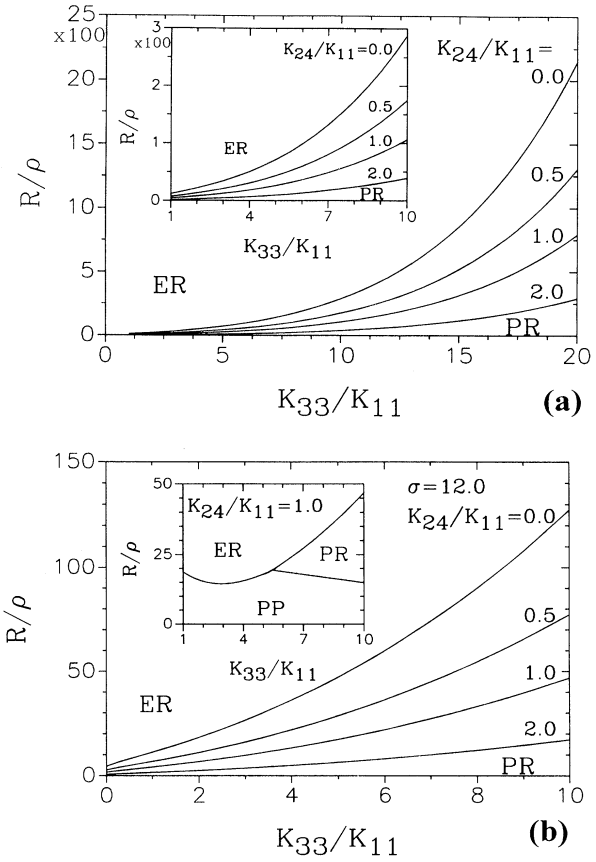

FIG. 3. A stability diagram of the escaped-radial and planar-radial nematic director fields in the strong (a) and weak (b) anchoring regimes; the inset of (b) shows the stability region for the planar-polar nematic director field when $K_{24}/K_{11}=1$.

escaped-radial structure with point defects (ERPD) is metastable, while, in short cylinders with planar anchoring conditions at the ends of the cylinder, structures with point defects are stable [28]. In a long cylinder, pairs of two types of defects, i.e., hyperbolic (negative) and radial (positive) defects separated by the average distance L, form a periodic configuration along the cylindrical axis with period $\sim 2L$. This situation is presented schematically in Fig. 1. The ERPD structures in long cylinders have been previously studied numerically [12] and with the use of trial solutions for equal elastic constants [10,11]. In this paper the study is extended to cases with $K_{33}/K_{11}\neq 1$.

IV. DEUTERIUM NMR MEASUREMENTS

In order to resolve the predicted effects, submicrometer cavities well below the resolution of an optical microscope are employed. In such cases deuterium NMR is an extremely useful technique to probe nematic director distributions [8–11, 29].

A macroscopic aligned bulk sample of a uniaxial liquid-crystal compound selectively deuterated will yield a spectrum of two lines separated by the frequency:

$$\delta\nu = \pm\tfrac{1}{2}\delta\nu_B(3\cos^2\theta_n - 1)\ , \tag{5}$$

where θ_n is the angle between the magnetic field and the local nematic director $\mathbf{n}$, and $\delta\nu_B$ is the maximum bulk quadrupole splitting frequency [30]. In the case of a confined nematic structure, $\theta_n = \theta_n(\mathbf{r})$, the spectrum shows a distribution of frequency shifts, $\delta\nu(\mathbf{r})$, which reflects the nematic director field. The extent of motional averaging can be estimated by comparing the distance the molecule migrates on the NMR time scale, $d \sim (D_t/\delta\nu_B)^{1/2}$, to the distance where the director changes appreciably. Using typical values of the translational diffusion constant $D_t \sim 10^{-11}\text{m}^2/\text{s}$, and the bulk quadrupole splitting frequency $\delta\nu_B = 50$ kHz, the distance the molecule diffuses is ~ 0.02 μm, which is significantly less than the employed cavity size. This allows us to neglect motional averaging [8].

The experimental spectral distribution is the Fourier transform of the free induction decay determined using well-known ^{2}H-NMR methods [31]. Because the ^{2}H-NMR spectra strongly depend on the parameters K_{33}/K_{11}, σ, and L/R, we first present a model analysis of their individual effect on the simulated line shapes. This will enable a reasonable data analysis in Sec. V. We first illustrate the influence of a diverging K_{33}/K_{11} ratio on the ^{2}H-NMR spectral patterns, by calculating the ideal defectless ER configurations for orientations of the cylinder axis parallel ($\theta_B = 0°$) and perpendicular ($\theta_B = 90°$) to the magnetic field, presented in Fig. 4. As can be seen here, radical changes in the spectra are observed when K_{33}/K_{11} diverges. In the strong anchoring regime [Fig. 4(a)], as K_{33}/K_{11} increases, the bend deformation becomes expensive, forcing the splay deformations to become dominant. The shoulders in the $\theta_B = 0°$ orientation decrease until it eventually reduces to a sharp doublet, indicating that the structure is planar ($K_{33}/K_{11} = \infty$). For the cylinder perpendicular to the field, however, the outer shoulders are increased when K_{33}/K_{11} is increased, approaching a classical cylindrical powder pattern [32] indicative of a PR structure ($K_{33}/K_{11} \to \infty$). In the weak anchoring regime [Fig. 4(b)], as K_{33}/K_{11} increases, the nematic director on the surface deviates away from the preferred homeotropic direction. The $\theta_B = 0°$ orientation shows the largest change of the quadrupole splitting frequency as the direction of the director on the surface passes through the magic angle [54.5° in Eq. (5)], ($K_{33}/K_{11} \sim 6.6$), where no splitting exists. For $K_{33}/K_{11} = 10$, a large contribution appears in the center of the spectrum as a consequence of the director field near the magic angle ($\sim 54.5°$). The $\theta_B = 90°$ orientation shows that the singularities corresponding to the $\theta = 0°$ director orientation are suppressed as K_{33}/K_{11} increases, as a direct consequence of the escaped region becoming more pronounced when the anchoring angle is enhanced.

In Fig. 5, we present the predicted NMR line shapes of nonideal escaped structures with point defects. The effect of the effective anchoring strength σ and the defect density L/R on the patterns corresponding to the ER structure with point defects in the vicinity of the nematic–smectic-A phase transition ($K_{33}/K_{11} = 7.0$) is shown (Fig. 5). Figure 5(a) contains the dependence of the spectra on the molecular anchoring strength via the parameter σ at a fixed point density ($L/R = 2$) and elastic constant ratio ($K_{33}/K_{11} = 7$). At weaker anchoring strengths more molecules align parallel to the cylinder axis, due to a large deviation of the molecular anchoring angle at the surface away from the homeotropic direc-

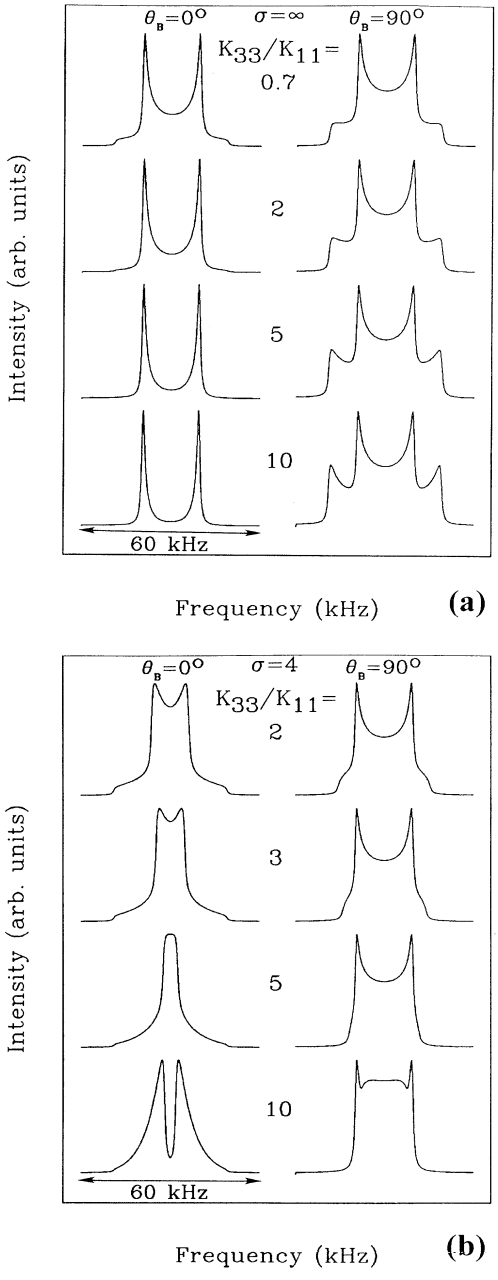

FIG. 4. Simulated ^{2}H-NMR spectral patterns for the escaped-radial configuration for parallel ($\theta_B = 0°$) and perpendicular ($\theta_B = 90°$) orientations of the cylinder axis in the magnetic field. The influence of K_{33}/K_{11} on the ^{2}H-NMR spectral patterns is demonstrated for strong ($\sigma = \infty$) and weak ($\sigma = 4$) anchoring in (a) and (b), respectively.

tion. For the $\theta_B = 90°$ cylinder orientation this is evident from the outer shoulders (which represent the molecules parallel to the field) decreasing as the effective anchoring strength is decreased. The calculated molecular anchoring angle Ω_R is shown in Fig. 6 as a function of the coordinate z (measured along the cylindrical axes) for $\sigma = 12$, $L/R = 2$, and $K_{33}/K_{11} = 1.8$, 3.0, 6.0, and 7.0. These values of σ and L/R will later be shown to be in accordance with those measured for our system. The molecular anchoring angle is perpendicular at points where planes perpendicular to the cylinder axis incorporating point defects intercept the cylindrical surface. The maximal deviation is in general not at the midpoint between the two defect planes at $z/L = \frac{1}{2}$, but depends on the value of K_{33}/K_{11}, because the radial defect is a pure splay defect (K_{11}) and the hyperbolic defect contains mostly bend deformation (K_{33}).

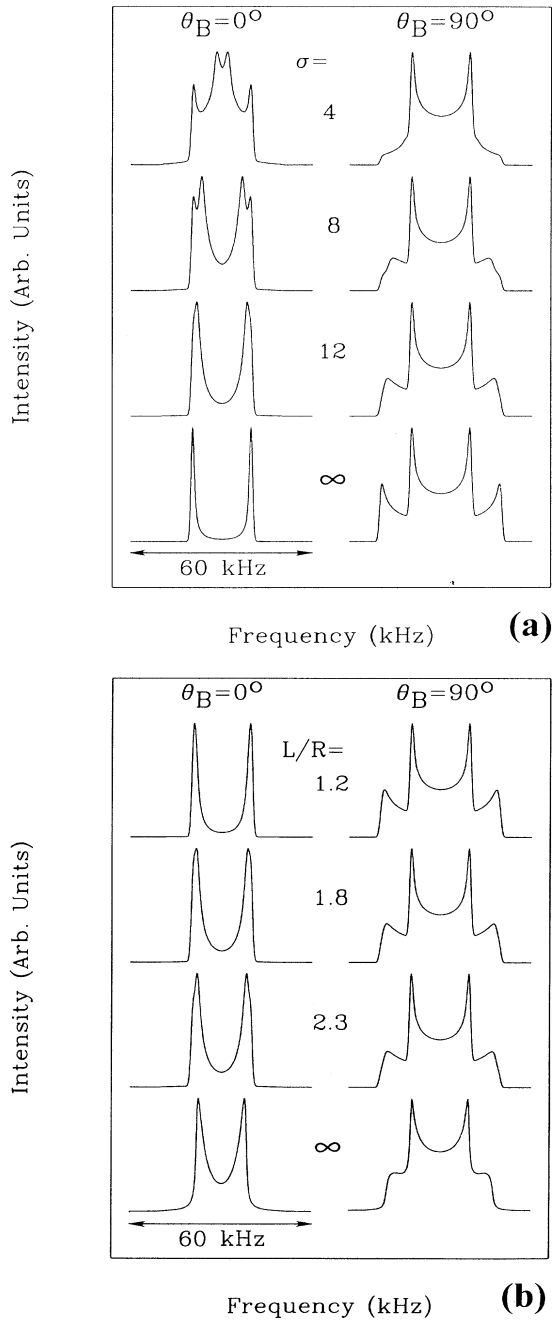

FIG. 5. Simulated ^{2}H-NMR spectral patterns for the escaped radial with point defects configuration for parallel ($\theta_B = 0°$) and perpendicular ($\theta_B = 90°$) orientations of the cylinder axis in the magnetic field. The influence of σ on the ^{2}H-NMR spectral patterns is demonstrated for $K_{33}/K_{11} = 7$ and $L/R = 2$ (a); and the influence of the point defect density is shown using $\sigma = 12$ and $K_{33}/K_{11} = 7$ (b).

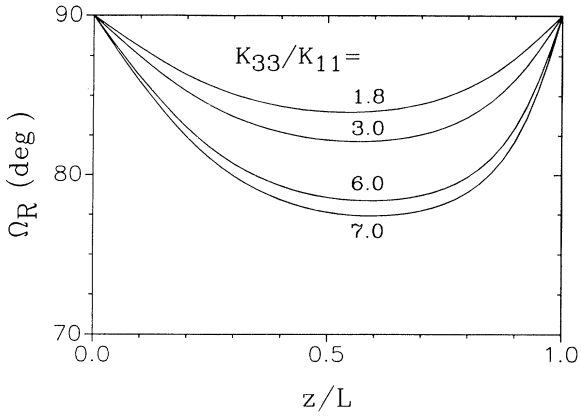

FIG. 6. The molecular anchoring angle profile at the cavity wall between successive defects for $\sigma = 12$ and various values of the K_{33}/K_{11} ratio.

The influence of the defect density L/R is represented in Fig. 5(b). For larger defect densities, i.e., smaller values of L/R, relatively more volume is occupied by nearly planar director fields. Decreasing the value of L/R gives the resulting NMR line shape more characteristics of the planar-radial structure, narrower $\theta = 90°$ peaks for the cylinder axis parallel to the field and larger $\theta = 0°$ peaks for the cylinder axis perpendicular to the NMR magnetic field [Fig. 5(b)].

V. DISCUSSION OF EXPERIMENTAL OBSERVATIONS

The 8CB confined to the $R = 0.1$ μm sample is studied for the cylinder axes parallel ($\theta_B = 0°$) and perpendicular ($\theta_B = 90°$) to the magnetic-field direction of the NMR spectrometer. Spectra were obtained as a function of decreasing temperature just below the isotropic phase transition temperature through the nematic phase. The spectra definitely show that liquid crystals in these cavities have escaped-radial director fields with a relatively large point defect density. The possible presence of planar (PP or PR) structures in a small number of cavities with below average radii [see phase diagram in Fig. 3(b)] cannot be ruled out.

Some typical experimental NMR line shapes (solid line) fitted to the simulated ones (dashed line) corresponding to ER structures with defects are shown in Fig. 7. The values of $K_{33}/K_{11} = 1.8$, 3.0, 6.0, and 7.0 used for

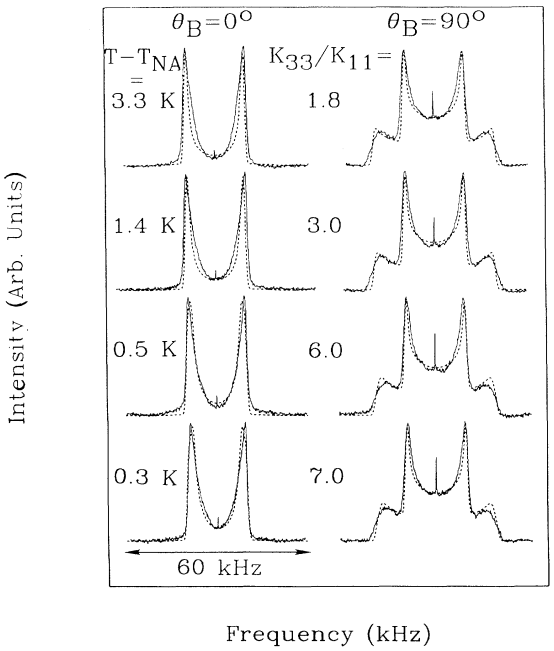

FIG. 7. ^{2}H-NMR spectra (solid line) of 8CB-βd_2 confined in $R=0.1$ μm cavities of Nuclepore membranes recorded at various temperatures fitted with simulated spectra (dashed line) using $\sigma=12$ and corresponding values of K_{33}/K_{11}.

spectra recorded at temperatures of 36.5, 34.5, 33.6, and 33.4 °C, respectively, were obtained from the literature [14]. Although the temperature dependence of the spectra is relatively subtle, we succeeded by choosing the best fits, to estimate $\sigma=12\pm1$ and $L/R=2.0\pm0.5$, independent of temperature. This temperature independence indicates the noncritical behavior of the physical parameters related to the quantities σ and L/R. It should be mentioned that we chose the previously reported values of K_{33}/K_{11} to have smaller uncertainty in determining σ and L/R, but in principle all three quantities can be simultaneously obtained by optimizing the fit of experimental spectra with theoretical NMR line shapes. The dependence of the director field on the value of K_{33}/K_{11} is strongest for the pure ER structure in both strong and weak (effective) anchoring regimes, as is shown in the line shapes of Figs. 4(a) and 4(b). For an intermediate value of the effective anchoring strength, $\sigma\sim12$, and a relatively high defect density $L/R=2$ (our case), the dependence of K_{33}/K_{11} is minimal, as can be seen in the line shapes of Fig. 7. We attribute this difference in the dependence on K_{33}/K_{11} mostly to the anchoring strength and to a lesser degree to the presence of the point defects. Retrieving the value of K_{33}/K_{11} from the simulated spectra fitted to the experimental line shapes, therefore, would be considerably more accurate if one were able to select a cavity radius or surface treatment so that the parameter σ would fall in one of the above-mentioned anchoring strength regimes. Let us analyze our results in detail.

A. Anchoring strength W_0

The relatively large value of $\sigma\sim12$ and the expectation that K_{24} has a comparable value, as in the similar compound 4'-pentyl-4-cyanobiphenyl (5CB) where $K_{11}\sim K_{24}$, indicates that in our case the effect of K_{24} is small. We can safely assume that $\sigma\sim RW_\theta/K_{11}$; however, in the same confining system using 5CB, σ was previously measured to be 4 ± 0.2. Taking this into account and using $K_{11}=6\times10^{-12}$ J/m for 8CB [33], $K_{11}=7\times10^{-12}$ J/m for 5CB and $R=0.1\times10^{-6}$ m, we find that the anchoring strength for 8CB on the polycarbonate surface is $(7\pm5)\times10^{-4}$ J/m^2, which is approximately 3.5 times larger than for 5CB. The stronger homeotropic orientational anchoring of longer liquid-crystal molecules is in agreement with the ordering study of Shen *et al.* [34]. They showed that coupling of cyanobiphenyl compounds (nCB) with a glass surface treated with silane, which induces homeotropic anchoring, increases as n increases.

B. Smectic layering

An attractive possibility to ascribe at least part of the large value of W_θ to the pretransitional smectic layering is ruled out since we found that the effective molecular anchoring strength $\sigma=12\pm1$ is roughly constant over the entire temperature range studied. According to our description of the layering effect (Sec. III), we can only conclude that $2D\xi<W_\theta\sim10^{-3}$ J/m^2. Knowing that $\xi(T_{NA}+0.2K)\sim0.05$ μm, we find $D<10^{-4}$ J/m^3, which is at least a factor of 100 smaller than the value reported by Rosenblatt for a glass surface [15]. Because $D\propto\Psi^2$, we can estimate that smectic order induced by polycarbonate surface is negligible (at least ten times smaller in comparison to glass surfaces). This behavior of the polycarbonate surface can be attributed to (i) a very weak positional anchoring, or (ii) surface roughness. Because the orientational anchoring strength is large, we believe that possibility (ii) is a consistent explanation. We can estimate the degree of roughness by equating the elastic energy density of a bend smectic layer $\frac{1}{2}K_{11}/r_c^2$ (r_c is the effective curvature of the layer) and $\frac{1}{2}a\Delta T$, the first term in a Landau expansion of the free energy of the smectic phase. Simply taking nematic values $K_{11}\sim10^{-11}$ J/m, $\Delta T\sim0.2$ K, $a\sim10^5$ J/m^3 K, we find $r_c=20$ nm as an estimate for the roughness of the polycarbonate surface. This is consistent with the previous electron scanning microscope studies, which were unfortunately limited in the resolution to details above 100 nm [20,29]. It was shown, at least on their scale, that the inner surface of cavities in such a polycarbonate matrix are rough and that they exhibit relatively pronounced concentric grooves.

C. Saddle-splay surface elastic constant K_{24}

As we mentioned above, the $\sigma=12$ value indicates small influences of K_{24} on the ER structures, and thus does not allow us to determine K_{24} directly from the NMR spectra. The value of σ and the absence of the transition to the PR structure with increasing K_{33}/K_{11} ratio in accordance with the stability diagram [Fig. 3(b)] limits the possible K_{24}/K_{11} ratio to values ≥1. Figure

3(b) shows that for our values of $K_{33}/K_{11}=7$, $\sigma=12\pm1$, and $R/\rho=20$, we are in the vicinity of the triple point.

D. Defect density

The temperature independence of L/R is in accordance with previous observations in similar systems [9–11], and is consistent with existing theories [12]. We believe the defect structures are strongly locked in by irregularities of the cavity surface.

VI. CONCLUSIONS

We have demonstrated the usefulness of ^{2}H-NMR to indirectly measure the dimensionless surface parameter $\sigma=RW_\theta/K_{11}+K_{24}/K_{11}-1$ to be ~12 for 8CB in the vicinity of the nematic–smectic-A phase transition. The determination of this parameter was achieved by fitting experimental spectra corresponding to the nematic liquid crystal confined in cylindrical cavities in polycarbonate membranes to predictions of elastic theory. The theoretical stability diagram for escaped-radial and planar-radial structures for $\sigma=12$ allowed us to estimate the lower bound for $K_{24}/K>1$ for 8CB.

Further, the value of W_θ is estimated to be $(7\pm5)\times10^{-4}$ J/m^2, which is 3.5 times larger than for a shorter cyanobiphenyl compound, 5CB. We interpret this relatively large value of W_θ as an increase in the surface coupling between the liquid-crystal molecule and the cavity wall as the length of the molecule increases.

Finally, the temperature independence of the anchoring strength, W_θ, indicates the lack of pretransitional smectic layering, contrary to reports in the literature for planar glass cells [15–17]. We attribute this result to the roughness (estimated to be $r_c=20$ nm) of the polycarbonate surface.

In the future this study is planned to be extended to systems with different surface treatments and radii that will allow a separate determination of K_{24} and W_θ by realizing the conditions where a transition from escaped-radial to planar-polar structures would occur.

ACKNOWLEDGMENTS

The National Science Foundation Solid State Chemistry Grant No. DMR091-20130 and the Ministry of Science and Technology of Slovenia are gratefully acknowledged. The 8CB-βd$_2$ was synthesized by S. Keast and M. Neubert.

*Permanent address: Department of Physics, University of Ljubljana, Jadranska 19, 61000 Ljubljana, Slovenia.

[1] P. E. Cladis and M. Kleman, J. Phys. (Paris) **33**, 591 (1972).
[2] R. B. Meyer, Philos. Mag. **27**, 405 (1973).
[3] A. Saupe, Mol. Cryst. Liq. Cryst. **21**, 211 (1973).
[4] C. E. Williams, P. Pieranski, and P. E. Cladis, Phys. Rev. Lett. **29**, 90 (1972).
[5] C. Williams, P. E. Cladis, and M. Kleman, Mol. Cryst. Liq. Cryst. **21**, 355 (1973).
[6] P. G. de Gennes, *The Physics of Liquid Crystals* (Clarendon, Oxford, 1974), and references therein.
[7] M. Kleman, *Points, Lines, and Walls in Liquid Crystals, Magnetic Systems, and Ordered Media* (Wiley, New York, 1988), and references therein.
[8] G. P. Crawford, M. Vilfan, I. Vilfan, and J. W. Doane, Phys. Rev. A **43**, 835 (1991).
[9] G. P. Crawford, D. W. Allender, M. Vilfan, I. Vilfan, and J. W. Doane, Phys. Rev. A **44**, 2570 (1991).
[10] G. P. Crawford, D. W. Allender, and J. W. Doane, Phys. Rev. A **45**, 8693 (1992); G. P. Crawford, Ph.D. dissertation, Kent State University, 1991 (unpublished).
[11] D. W. Allender, G. P. Crawford, and J. W. Doane, Phys. Rev. Lett. **67**, 1442 (1991).
[12] I. Vilfan, M. Vilfan, and S. Žumer, Phys. Rev. A **43**, 6875 (1991).
[13] P. E. Cladis, Philos. Mag. **29**, 641 (1974).
[14] H. Hakemi, Liq. Cryst. **5**, 334 (1989).
[15] C. Rosenblatt, Phys. Rev. Lett. **53**, 791 (1984).
[16] B. M. Ocko, A. Braslau, P. Pershan, J. Als-Nielsen, and M. Deutsch, Phys. Rev. Lett. **57**, 94 (1986).
[17] B. M. Ocko, Phys. Rev. Lett. **64**, 2160 (1990).
[18] S. Keast and M. Neubert (private communication).
[19] Nuclepore Corporation, 7035 Commerce Circle, Pleasanton, CA 94566.
[20] G. P. Crawford, L. M. Steele, R. Ondris-Crawford, G. S. Iannacchione, C. J. Yeagar, J. W. Doane, and D. Finotello, J. Chem. Phys. **96**, 7788 (1992).
[21] T. P. Chen, M. J. Dipirro, B. Bhattacharyya, and F. M. Gasparini, Rev. Sci. Instrum. **51**, 846 (1980).
[22] M. Kuzma and M. M. Labes, Mol. Cryst. Liq. Cryst. **100**, 103 (1983).
[23] G. Barbero and Barberi, in *Physics of Liquid Crystalline Materials,* edited by I. C. Khoo and F. Simoni (Gordon and Breach, Philadelphia, 1991), Chaps. VIII and IX.
[24] A. Rapini and M. Papoular, J. Phys. (Paris) Colloq. **30**, C4-C5 (1969).
[25] T. G. Lubensky, J. Chim. Phys. (Paris) **80**, 31 (1983).
[26] E. Dzyaloshinskii, Zh. Eksp. Teor. Fiz. **31**, 773 (1970) [Sov. Phys. JETP **33**, 773 (1970)].
[27] S. Kralj and S. Žumer (unpublished).
[28] Shu-Hsia Chen and B.-J. Liang, Appl. Phys. Lett. **59**, 1171 (1991).
[29] R. J. Ondris-Crawford, G. P. Crawford, S. Žumer, and J. W. Doane, Phys. Rev. Lett. **70**, 194 (1993).
[30] J. W. Doane, in *Magnetic Resonance of Phase Transitions,* edited by F. J. Owens, C. P. Poole, Jr., and H. A. Farach (Academic, New York, 1979), Chap. 4.
[31] A. Abragam, *The Principle of Nuclear Magnetism* (Oxford University Press, London, 1961).
[32] G. Chidichimo, Z. Yaniv, N. P. Vaz, and J. W. Doane, Phys. Rev. A **25**, 25 (1982).
[33] Stephen W. Morris, P. Palffy-Muhoray, and D. A. Balzarini, Mol. Cryst. Liq. Cryst. **139**, 263 (1986).
[34] W. Shen, L. J. Martinez-Miranda, H. Hsiung, and Y. R. Shen, Phys. Rev. Lett. **62**, 1860 (1989).